DISCLAIMER NOTICE

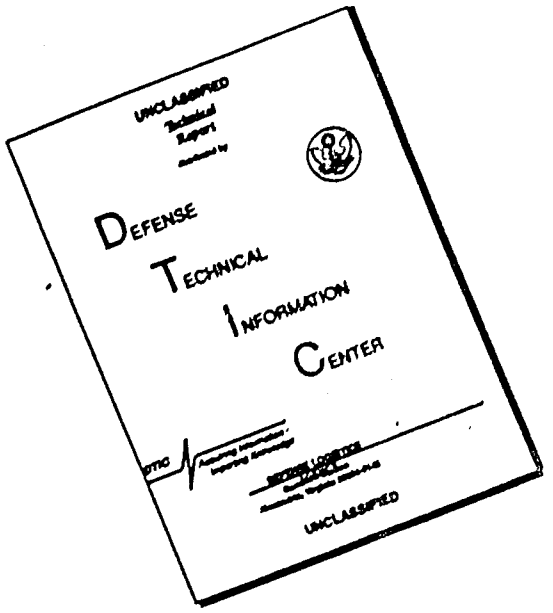

THIS DOCUMENT IS BEST QUALITY AVAILABLE. THE COPY FURNISHED TO DTIC CONTAINED A SIGNIFICANT NUMBER OF PAGES WHICH DO NOT REPRODUCE LEGIBLY.

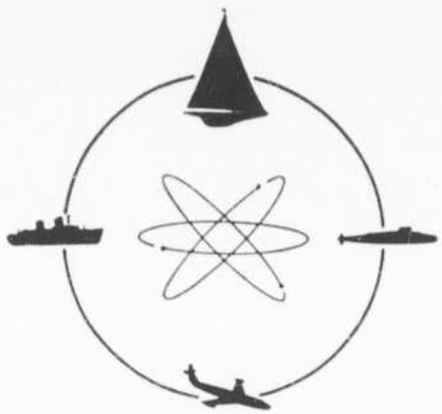

DAVIDSON LABORATORY

STEVENS INSTITUTE
OF TECHNOLOGY

CASTLE POINT STATION
HOBOKEN, NEW JERSEY

QUARTERLY PROGRESS REPORT JANUARY - MARCH 1961

RESEARCH PROGRAM ON CONVERSION OF EXPLOSIVE ENERGY

Contract DA-28-017-501-ORD-3450
DL Project LB-2221

STEVENS INSTITUTE OF TECHNOLOGY
DAVIDSON LABORATORY
CASTLE POINT STATION
HOBOKEN, NEW JERSEY

QUARTERLY PROGRESS REPORT JANUARY - MARCH 1961

RESEARCH PROGRAM ON CONVERSION OF EXPLOSIVE ENERGY

Contract DA-28-017-501-ORD-3450
DL Project LB-2221

Prepared by: S J Lukasik

S.J. Lukasik, Head
Fluid Physics Division

TABLE OF CONTENTS

Quarterly Progress Report January - March 1961
Research Program on Conversion of Explosive Energy

Contract DA-28-017-501-ORD-3450
DL Project LB-2221

SCOPE OF WORK

Efforts during the first quarter of 1961 have been largely directed toward the analysis of existing data and the construction of equipment for future work. No new firings are reported here. Some of the measured conductivity values have been revised in the light of more complete probe calibration data. A complete tabulation of conductivity probe characteristics is included as an appendix. The main new results have consisted of a careful study of the conductivity circuit rise time and the effect of signal cable length and circuit parameters on the observed signal. This has resulted in a considerably greater confidence in the reported conductivity values. However, it has also indicated that the observed signal cannot be interpreted so closely as to yield detailed information on the structure of the reaction zone.

The design of the capacitor bank is complete and the construction is well-advanced. The bank consists of two rings of ten capacitors feeding a central load. It was decided that low inductance coaxial cable would offer considerable advantages in cost and convenience over two or three-element parallel plate transmission lines without an undue inductance penalty. A connection of sufficiently low inductance was designed to couple the capacitors to the central collector plate which is connected to the load coil by a two-element transmission line. Switching is provided by an air-gap whose breakdown is initiated at three points by a 10 kv pulse. Present estimates are that the total bank inductance will be about 9mμh; the self-inductance of the capacitors account for 2mμh, while the connections, cabling, lines, switch and collector plate make up the remainder. This indicates that the bank efficiency will be about 85% for a 50mμh load such as has been used in the past and will be 53% for a load as small as 10mμh.

Further design and initial tests of the vacuum system for the shaped charge jet collisions have been carried out for the purpose of settling on the pump, valve, gauge and manifold requirements.

A paper "Electrical Resistivity During a Detonation" by S. Koslov, S.J. Lukasik, and B.J. Pernick was read before the meeting of the American Physical Society held in New York City, 1-4 February 1961.

RESULTS OF WORK

A. Magnetic Field Work

In this quarter, the design of the new capacitor bank was completed and construction was begun. A circular layout of capacitors was chosen for the bank. In this arrangement the capacitors are stacked in units of two on separate frames, which are then bolted to each other to form a circle, (see Fig. 1). The capacitors, instead of being connected by parallel plate transmission paths, will be connected by low inductance coaxial cable into a central collector plate. To this collector plate is connected the spark gap and load coil.

In order to deposit as much as possible of the energy stored in the capacitors into the load coil, it is necessary that the bank have an internal inductance that is small compared to the inductance of the load coil. The efficiency of the bank is given by

$$e = \frac{L_{\ell c}}{L_i + L_{\ell c}} ,$$

where $L_{\ell c}$ is the inductance of the load coil and L_i is the internal inductance of the bank. The internal bank inductance L_i can be decomposed into the inductance of the spark gap switch (L_{sg}), the inductance of the collector plate (L_{cp}), the inductance of the transmission line from the collector plate to the spark gap $(L_{t\ell})$, the parallel equivalent of the inductance of the coaxial cables (L_{cc}), the parallel equivalent of the inductance of the cable-to-capacitor connection (L_{co}) and finally the parallel equivalent of the internal inductance of the capacitors (L_c).

For the present bank, the nominal internal inductance of each capacitor is 40 mμh and there are 20 capacitors. Therefore,

$$L_c = \frac{40 m\mu h}{20} = 2.0 m\mu h .$$

The coaxial cable is connected to each capacitor by means of two clamps connected to parallel plates which are made to fit the contour of the capacitor terminals (see Fig. 2). These two parallel plates are insulated by a layer of mylar 0.010 in. thick. The major contribution to the inductance of the connection arises from the geometry of a cylinder parallel to

Figure 1

Two capacitors on frame

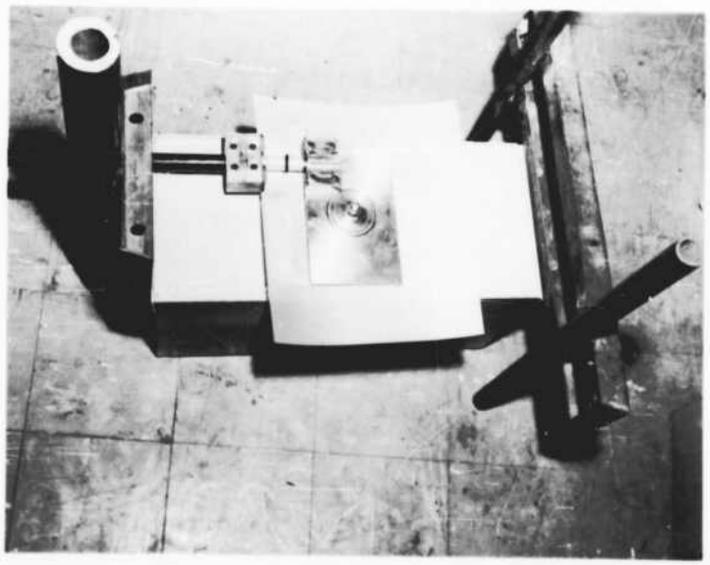

Figure 2

Cable termination at capacitor

a plane. The inductance of such a geometry is given approximately by[1]

$$L = 0.01016\,\ell\left[\ln\left(\frac{2D}{d}\right) - \frac{D}{\ell} + \frac{1}{4}\right]\mu h \ .$$

for ℓ in in.

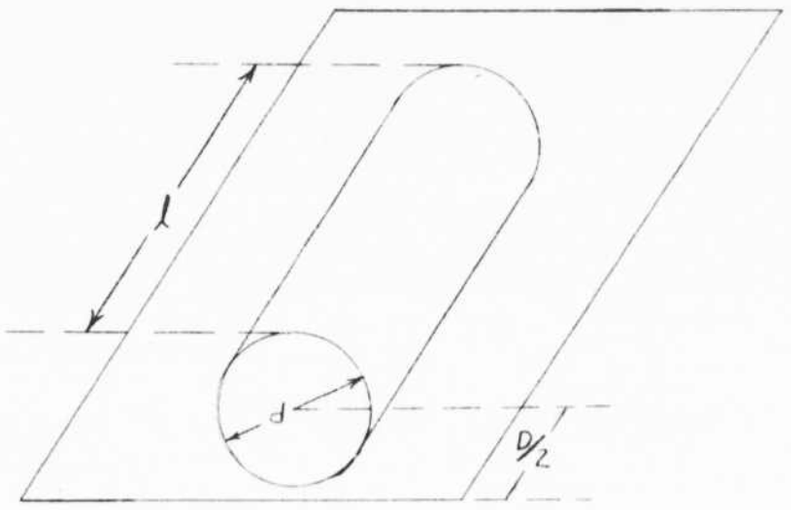

For ℓ = 2.25 in., d = 0.725 in., and D/2 = 0.512 in., L = 19 mμh.

Therefore

$$L_{co} = \frac{19 m\mu h}{20} = 0.95\ m\mu h \ .$$

The length of coaxial cable between each capacitor and the collector plate is about 16 in. Since the cable inductance is 6mμh/ft,

$$L_{cc} = 6 m\mu h/ft \times 4/3\ ft \times \frac{1}{20} = 0.4 m\mu h \ .$$

The collector plate consists of two concentric circular plates separated by 0.010 in. mylar sheet for insulation. Along the rims of these plates are rings to terminate the coaxial cable (see Fig. 3). These rings are separated by 1 in. in order to hold off the voltage. For ℓ = 1 in., d = 0.725 in. and D/2 = 0.512 in., the cylinder-to-plane inductance of each connection is 2.69mμh. Thus the equivalent inductance for 20 such

---

(1) F.W. Grover "Inductance Calculations", D. Van Nostrand Co. (1946)

connections is 0.13mμh. By considering current paths from the cables, the inductance between the circular plates is estimated to be about 0.75mμh. Hence the total inductance of the collector plate

$$L_{cp} = 0.13 + 0.75 = 0.9m\mu h .$$

Two flanges forming a transmission lines 5 in. wide and 2 ft long will lead from the collector plate to the spark gap assembly. For a plate separation of .015 in., the inductance $L = \mu_o \ell h/b$, for ℓ = 2 ft, h = 0.015 in., and b = 5 in., is equal to 2.30mμh. That is

$$L_{t\ell} = 2.30m\mu h$$

To minimize the inductance of the spark gap assembly, three separate spark gaps are placed in parallel (see Fig. 4). Then, assuming that they all fire simultaneously, the equivalent inductance will be reduced to 1/3 the inductance of one spark gap and the magnetic field in the gap will be more uniform

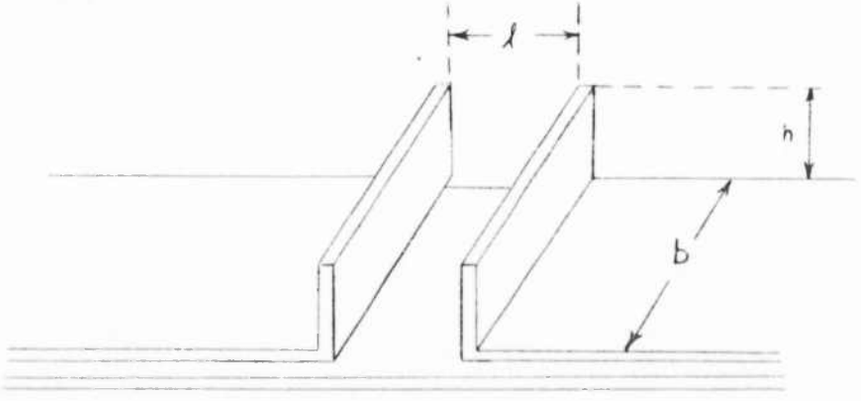

From the sketch above, the flux $\phi = B\ell h = LI$, and by Ampere's law, $Bb = \mu_o I$, assuming a uniform field in the air gap. Therefore, $L = \frac{\mu_o \ell h}{b}$; for b = 5 in., ℓ = 0.4 in., and h = 1 in., the spark gap inductance is

$$L_{sg} = 2.6m\mu h .$$

These inductance calculations are summarized in Table I below.

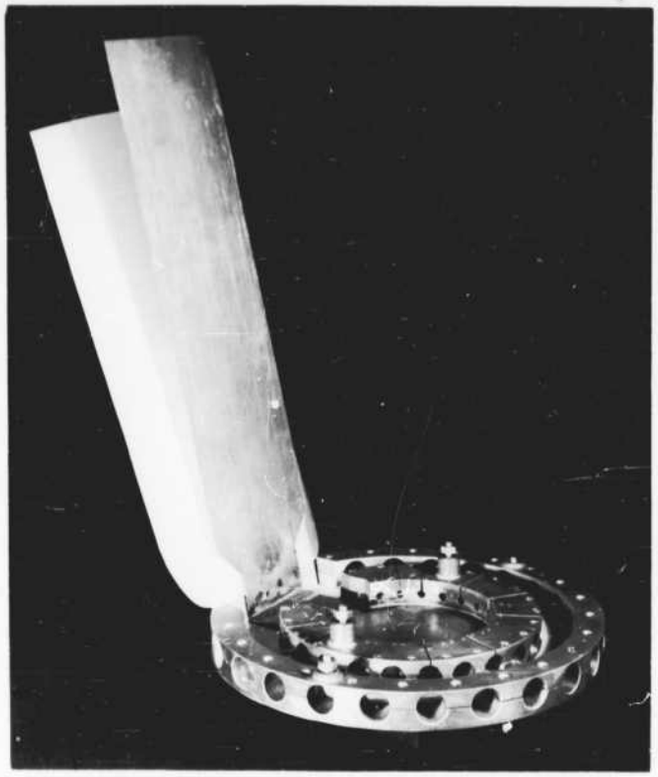

Figure 3

Collector plate and transmission line to spark gap switch

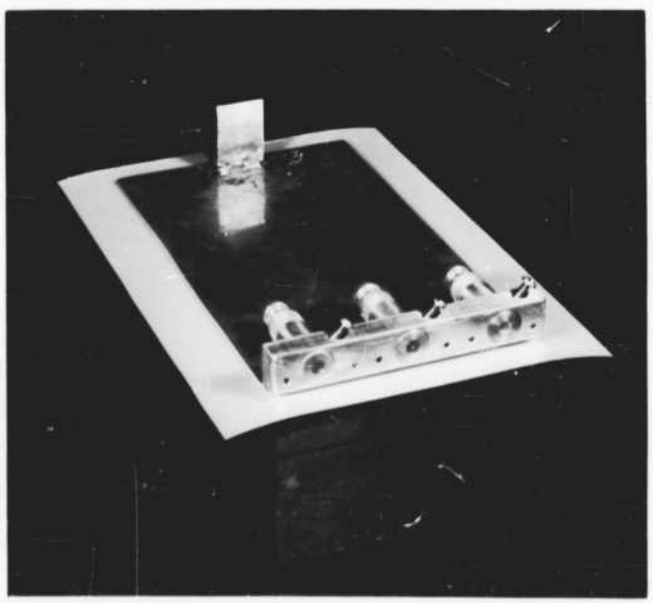

Figure 4

Spark gap switch and load coil

TABLE I

Design Estimates of Capacitor Bank Inductance

Item	Unit Inductance	No. of Units	Total Inductance
Capacitor L_c	40mμh	20	2.0mμh
Cable connection L_{co}	19	20	1.0
Coaxial cable L_{cc}	8	20	0.4
Collector plate L_{cp}	0.9	1	0.9
Transmission line $L_{t\ell}$	2.3	1	2.3
Spark gap switch L_{sg}	2.6	1	2.6

The sum of these internal bank inductances is approximately 9.2mμh.

The period of the system is given by

$$\tau = 2\pi \left[(L_i + L_{\ell c})C \right]^{1/2}$$

Where C = capacitance of bank = 180μf. Table II summarizes estimates of the bank efficiency and the quarter-period for various load coil inductances assuming an internal inductance of 9.2mμh.

TABLE II

Estimates of Bank Efficiency and System Quarter Period

Load Coil Inductance L_c	Efficiency e	Quarter Period $\tau/4$
30mμh	76.5%	4.2 μs
50	84.5	5.1
70	88.4	5.9
90	90.7	6.6

B. Conductivity Measurement

(a) Introduction During this quarter emphasis was directed towards an analysis of the conductivity circuitry and confirmatory laboratory experiments. The final intent of such a program is to provide a rational basis for calculating conductivity probe resistance, and hence, resistivity, in a transient explosive environment. During the course of this work, some instrumentation modifications for improved performance have become apparent.

(b) Transmission line analysis Due to the very short time duration in which the detonation zone sweeps across the conductivity probes and the long lengths of signal cable used in connecting electrical components, the propagation characteristics of the cable must be included in any interpretation of the observed electrical conductivity signals. Ordinary transmission line theory[1] is used in determining the signal time-dependence upon characteristic cable parameters and the variation of conductivity signal output with resistive load at the end of the cable. The results are outlined below.

The conductivity circuit is shown schematically below. The battery, V_o, capacitor, C, resistor r are representative of components used in the actual circuit. For purposes of analysis the conductivity probe is characterized as a resistance element, R, and a switch, S, the switch being closed when the detonation front shorts the probe tips. The characteristic impedance of the cable is Z_o.

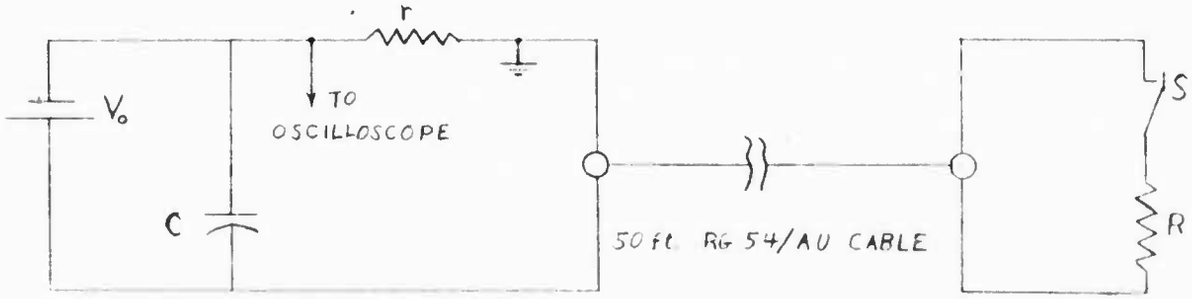

As will be shown later effects due to the capacitor, C, and the internal impedance of the battery can be neglected.

The sequence of events is as follows. Initially the cable is charged to a voltage, $-V_o$. When S is closed a pulse of height Δ travels down the cable towards the resistor r. After a time τ, this pulse will reach the end of the cable where a fraction of the pulse, k_r, will be reflected back up the cable towards the resistor R, and the remainder will appear across r. The reflected pulse will reach the beginning of the cable after a time 2τ, when again, a part, k_R, will be reflected down the cable, the remaining part being absorbed by the terminating resistor, R. The second

---

(1) S.L. Stewart "Circuit Analysis of Transmission Lines", J. Wiley (1958)

pulse to travel down the cable will arrive at the resistor r after a time 3τ where again a fraction, k_r, will be reflected up the cable, the remainder absorbed by the resistor r. The cycle repeats in time until a steady state is established.

If $e_s(t)$ represents the signal voltage across the measuring resistor r then one has the following sequence

$$e_s(t) = 0 \qquad 0 \leqslant t < \tau \tag{1}$$

$$e_s(t) = \Delta - k_r\Delta \qquad \tau \leqslant t < 3\tau \tag{2}$$

$$e_s(t) = \Delta - k_r\Delta + k_rk_R\Delta - k_r^2k_R\Delta \qquad 3\tau \leqslant t < 5\tau \tag{3}$$

Evaluating these expressions in terms of circuit parameters one has

$$\Delta = \frac{V_o Z_o}{Z_o + R} \tag{4}$$

$$k_r = \frac{Z_o - r}{Z_o + r} \tag{5}$$

$$k_R = \frac{Z_o - R}{Z_o + R} \tag{6}$$

Hence

$$e_s(t) = \frac{V_o Z_o}{Z_o + R} \frac{2r}{Z_o + r} \qquad \tau \leqslant t < 3\tau \tag{7}$$

$$e_s(t) = \frac{V_o Z_o}{(Z_o + R)^2} \frac{4r\,(Z_o^2 + rR)}{(Z_o + r)^2} \qquad 3\tau \leqslant t < 5\tau \tag{8}$$

The transit time τ can be written as

$$\tau = \sqrt{L_c C_c}\; d \tag{9}$$

where L_c, C_c are the inductance and capacity per unit length of cable and d is the total length of cable. For a typical length of 50 ft of RG 5U/AU cable, τ is $7.5 \times 10^{-2}\,\mu$sec.

Equations (7) and (8) can be expressed non-dimensionally as

$$\frac{e_s(t)}{V_o} = \frac{2}{(1 + R/Z_o)(Z_o/r + 1)} \qquad \tau \leqslant t < 3\tau \tag{10}$$

$$\frac{e_s(t)}{V_o} = \frac{4(Z_o/r + R/Z_o)}{(1 + R/Z_o)^2(1 + Z_o/r)^2} \qquad 3\tau \leqslant t < 5\tau \tag{11}$$

For a properly terminated line, $r = Z_o$, equations (10) and (11) both reduce to

$$\frac{e_s(t)}{V_o} = \frac{1}{(1 + R/Z_o)} = \frac{1}{(1 + R/r)} \qquad t \geqslant \tau \tag{12}$$

That is, the signal voltage, e_s, reaches its final value upon arrival of the first (and only) pulse.

Equations (10) and (11) were evaluated for r equal to 20 ohm and Z_o equal to 58 ohm, values that are appropriate to components used in the conductivity circuitry. The results are shown in Fig. 5, along with a plot of equation (12) for comparison.

(c) Effect of supply capacitor and battery resistance To show that the capacitor, C, and internal battery resistance can be neglected for the time interval over which the explosive conductivity measurements are observed, consider the following schematic representation of the conductivity circuitry.

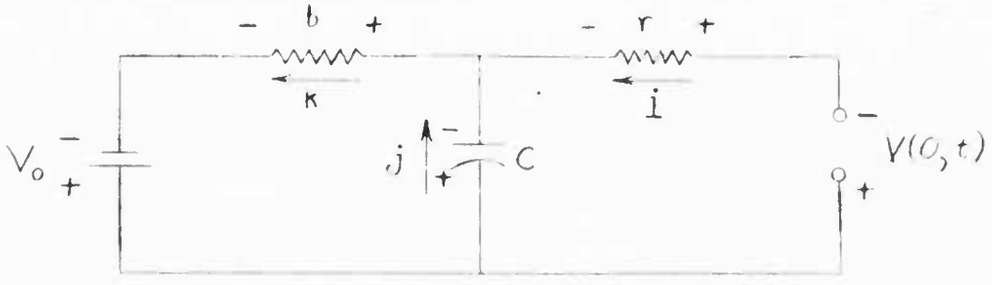

The branch currents are labeled i, j, k; b represents the internal resistance of the battery, V_o; and $V(0,t)$ represents the voltage across the end of the cable at a time t. The capacitor is charged to an initial voltage, V_o, where

$$Q_o = C V_o$$

For the time interval $0 \leqslant t < \tau$ one has

$$V(0,t) = V_o$$

Thus all branch currents are zero and the output signal e_s, equal to the voltage drop ir, is also zero.

Figure 5

Variation of output signal voltage with cable load resistance

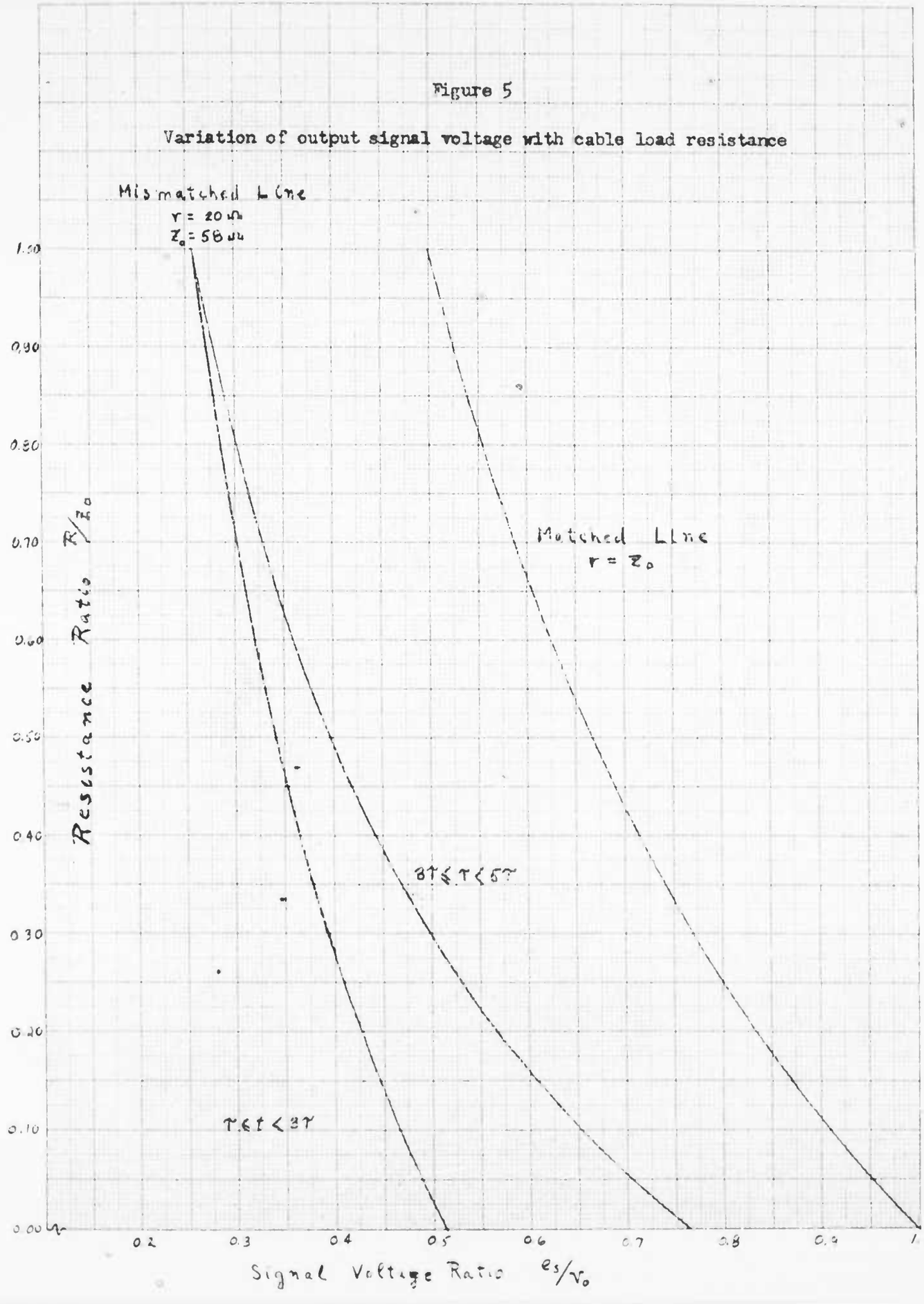

For the time interval $\tau \leqslant t < 3\tau$ the cable voltage drops to

$$V(0,t) = V_o - (\Delta - k_r\Delta)$$

The circuit equations are

$$V_o = k\,b + i\,r + V(0,t)$$

or

$$k\,b + i\,r = (\Delta - k_r\Delta)$$

Also

$$\frac{q - Q_o}{C} + i\,r = V(0,t)$$

where

$$\frac{dq}{dt} = j$$

and

$$i + j = k$$

Solving the above equations for i

$$\frac{di}{dt} + \frac{r+b}{rbC}\left[i - \frac{(\Delta - k_r\Delta)}{r+b} \right] = 0$$

Integrating

$$i = \frac{\Delta - k_r\Delta}{r+b} + \text{Const}\, e^{-\left(\frac{r+b}{rbC}\right)t}$$

Making the reasonable assumption that $r \gg b$;

$$i = \frac{(\Delta - k_r\Delta)}{r} + \text{Const}\, e^{-\frac{t}{bC}} \qquad (13)$$

The constant in equation (13) is determined from the condition that

$$q = 0 \quad \text{at} \quad t = \tau$$

Solving for the constant

$$\text{Constant} = -\frac{b}{r^2}(\Delta - k_r\Delta)e^{\tau/bC}$$

Hence, equation (13) becomes

$$i = \frac{(\Delta - k_r \Delta)}{r} \left(1 - \frac{b}{r} e^{-\frac{t-\tau}{bC}}\right) \qquad (14)$$

In order that the observed signal, e_s, be just the net cable pulse height, $\Delta - k_r \Delta$, the second term in equation (14), expressing a dependence upon the capacitor, C, and resistance, b, must be small enough to be neglected. Now, the time duration of concern is

$$0 \leqslant t - \tau < 2\tau$$

The exponential term has its maximum value when $t - \tau$ is zero. Hence the second term is of order b/r. Typical values of b for storage batteries range from 0.01 to 0.001 ohm in magnitude. For r equal to 20 ohm the ratio is

$$\frac{r}{b} \sim 0.5 \text{ to } 0.05\%$$

Thus, neglecting the effect of the capacitor, C, and of battery resistance, b, is of small consequence.

In a majority of firings, the battery was removed just prior to firing. For this situation the effect of the capacitor C can also be neglected, as is shown below. The circuit schematic pertaining to this case is

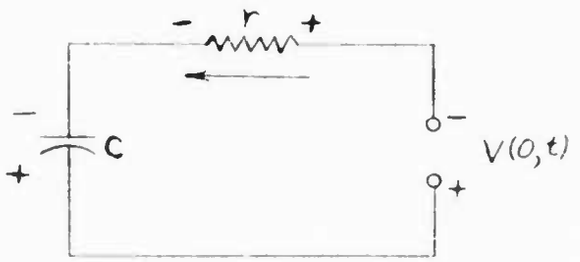

Thus

$$\frac{q - Q_o}{C} + i\,r = V(0,t) = -V_o + (\Delta - k_r \Delta)$$

Hence $\frac{dq}{dt} + \frac{q}{rC} = \frac{(\Delta - k_r \Delta)}{r}$

Solving for q

$$q = C(\Delta - k_r \Delta)\left(1 - e^{-\frac{t-\tau}{rC}}\right)$$

The current i is

$$i = \frac{dq}{dt} = \frac{(\Delta - k_r \Delta)}{r} e^{-\frac{t-\tau}{rC}}$$

The maximum deviation of the signal voltage ir from $(\Delta - k_r \Delta)$ occurs for $t-\tau$ equal to 2τ. Now 2τ is of the order of $0.20\,\mu s$ for the length of cable used in the circuit. The time constant rC is

$$rC = (20\ \Omega)(10^3\ \mu f) = 2 \times 10^4\ \mu sec$$

Hence the exponential term

$$e^{-\frac{2\tau}{rC}} \simeq e^{-10^{-5}} \simeq 1$$

Thus the effects due to C are negligible for time durations, 2τ, small compared to the time constant, rC.

(d) Laboratory experiments with a known resistor A number of laboratory experiments using a fixed resistor for a load resistance, R, were performed to exhibit and verify some of the relations given above and to determine the nature of the initial oscillating signal observed when recording explosive resistances. Specifically, variations of signal characteristics with r, R, and cable lengths were sought. In order to simulate as closely as possible actual operating conditions, the circuitry used for conductivity firings with identical lengths of connecting cable were also used in these measurements. To simulate the rapid onset of conduction in a detonation zone, a mercury relay switch was placed in series with the load, R. The complete electrical circuit is shown below:

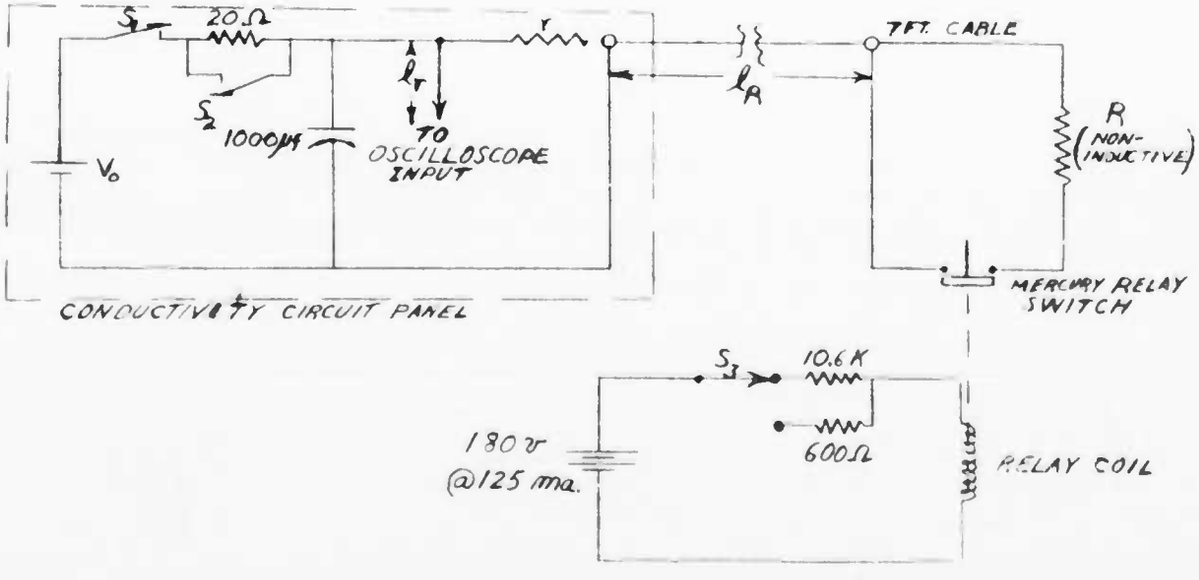

The 1000μf capacitor is charged through 20 ohms by closing switch S_1. To complete charging, the 20 ohm resistor is shorted by switch S_2. The battery is then removed from the circuit by reopening S_1. Switch S_3 controls the position of the mercury switch, and is shown in a normally open position. The output signal across r was displayed upon a Tektronix type 555 oscilloscope, the sweep trigger being initiated from the signal. Lengths of cable connecting the circuit panel with R, and with the oscilloscope input terminal are labeled ℓ_R and ℓ_r respectively, RG 54/AU cable being used throughout.

To facilitate discussion, the results will be presented so that the effects of varying one of the quantities r, R, ℓ_R, or ℓ_r at a time will be explicit.

Variation of signal resistor r Results obtained using two values of r are given in Table III. The calculated signal voltage, e_s, is obtained from equation (10); the calculated round trip transit time, 2τ, is obtained from equation (9) using a total cable length of $\ell_R + \ell_r$ ft. The frequency of the superposed oscillations on the observed signal is labeled f. Reproductions of the oscilloscope traces are shown in Figs. 6(a) and 6(b). The first case approximates values found in explosive measurements. The second illustrates the effect of terminating the cable with a resistance value close to the 50 ohm cable impedance.

TABLE III

Effect of Variation of Signal Resistor, r

r (ohm)	R (ohm)	ℓ_R (ft)	ℓ_r (ft)	Meas. e_s (volt)	Calc. e_s (volt)	Meas. 2τ (μs)	Calc. 2τ (μs)	f (mc)
20	20	57	5	4.3	4.1	0.20	0.18	15
60	20	57	5	8.6	8.3	0.20	0.18	15

The signal amplitude rises more rapidly towards its final value for the second case since the line is closely matched, i.e., the reflection coefficient, k_r, is very small. Due to the superposed oscillation upon the voltage step, an average voltage height was read. Nevertheless, there is good agreement between calculated and measured voltage values. The corresponding values for the round-trip transit time 2τ, are substantially in agreement.

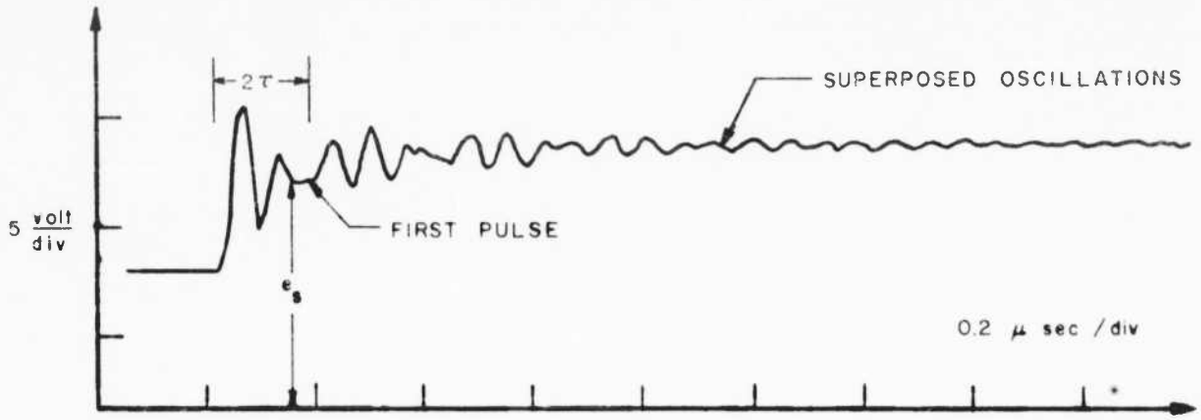

FIGURE 6 a MISMATCHED LINE ($r = Z_o$)

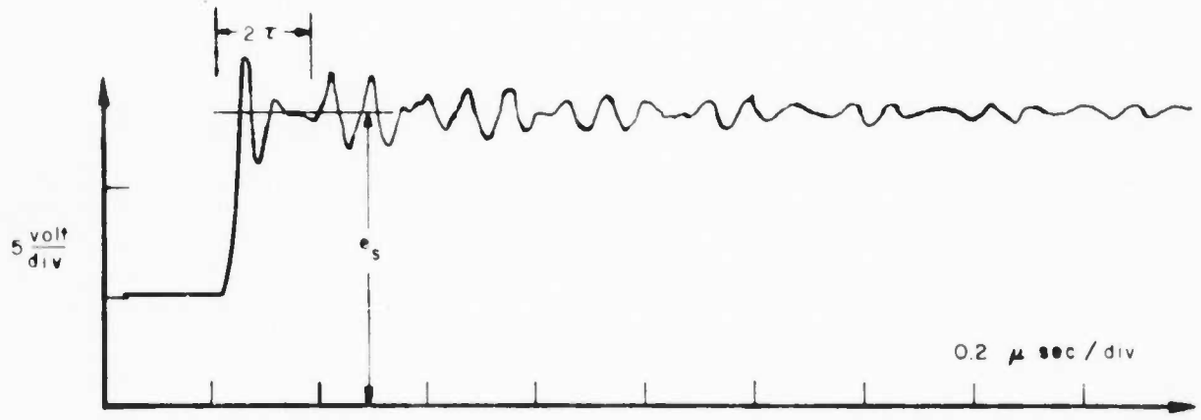

FIGURE 6b MATCHED LINE ($r = Z_o$)

FIGURE 6. TYPICAL SIGNAL RECORDS (SEE TABLES III, IV)

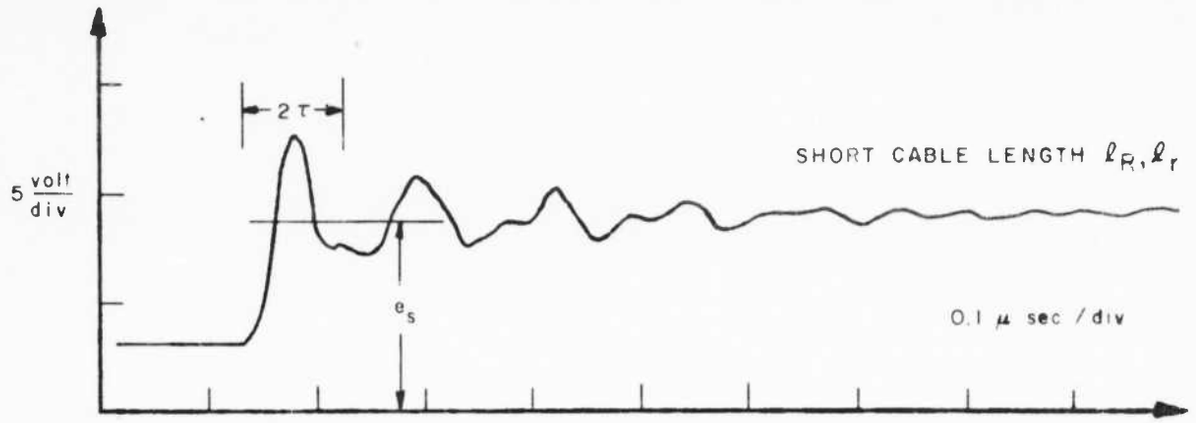

FIGURE 7. TYPICAL SIGNAL RECORD (SEE TABLE V)

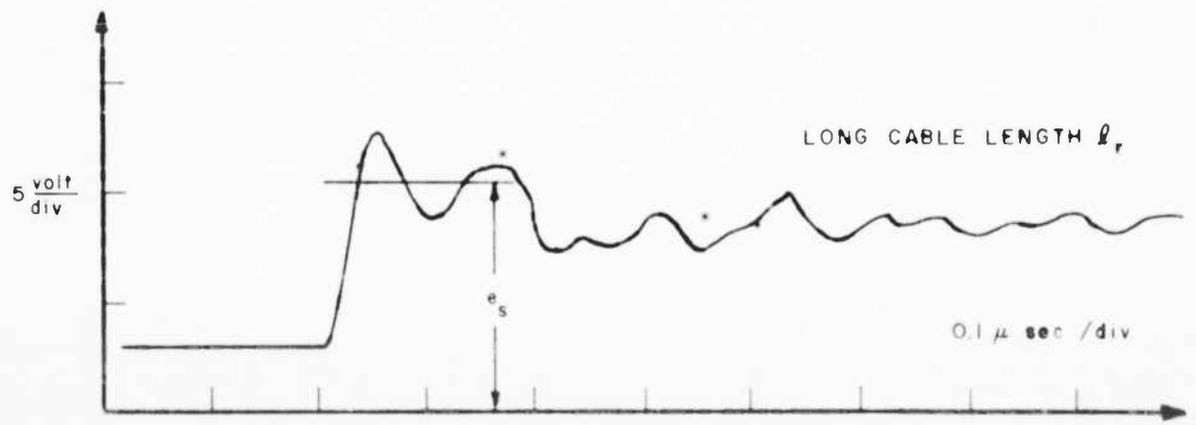

FIGURE 8. TYPICAL SIGNAL RECORD (SEE TABLE VI)

Variation of load resistor R Results obtained using two values of R are shown in Table IV; the corresponding oscilloscope traces are similar in shape and content to that of Fig. 6(b)

TABLE IV

Effect of Variation of Load Resistor, R

r (ohm)	R (ohm)	ℓ_R (ft)	ℓ_r (ft)	Meas. e_s (volt)	Calc. e_s (volt)	Meas. 2τ (μs)	Calc. 2τ (μs)	f (mc)
60	20	57	5	8.6	8.3	0.20	0.18	15
60	57.5	57	5	5.9	5.6	0.22	0.18	15

Again, the effect of proper cable termination is apparent in both situations and, as before, both the signal voltage and the transit time values are in agreement.

Variation of cable length ℓ_R Results pertaining to the use of two different cable lengths are shown in Table V. A reproduction of the oscilloscope trace for the second case is shown in Fig. 7; the trace corresponding to the first case is typically that of Fig. 6(b)

TABLE V

Effect of Variation of Cable Length, ℓ_R

r (ohm)	R (ohm)	ℓ_R (ft)	ℓ_r (ft)	Meas. e_s (volt)	Calc. e_s (volt)	Meas. 2τ (μs)	Calc. 2τ (μs)	f (mc)
60	57.5	57	5	5.9	5.6	0.22	0.18	15
60	57.5	14	5	5.0	5.6	0.10	0.06	20

As before the effect of proper termination and the good agreement between values of the signal voltage are apparent. The reason for the change in measured signal voltage with cable length is not apparent. Since the oscillatory signal did not go through a complete half cycle, the frequency value of 20 mc may be in error. The increasing discrepancy in transit time values may indicate a threshold dependence of τ upon cable length, and may be due to other parasitic contributions.

Variation of cable length ℓ_r Results related to the use of two different cable lengths are shown in Table VI. The corresponding oscilloscope traces are shown in Figs. 7 and 8.

TABLE VI

Effect of Variation of Cable Length, ℓ_r

r (ohm)	R (ohm)	ℓ_R (ft)	ℓ_r (ft)	Meas. e_s (volt)	Calc. e_s (volt)	Meas. 2τ (μs)	Calc. 2τ (μs)	f (mc)
60	57.5	14	5	5.0	5.6	0.10	0.06	20
60	57.5	14	50	7.5	5.6	0.16	0.19	10

Figure 8 shows a number of features not seen previously. First, there is much signal distortion, both in the oscillatory signals and in the regions corresponding to a pulse plateau. Secondly, the initial average signal voltage is greater than all other pulses on the trace. Finally, there is a significant difference between measured and calculated transit times for the two different cable lengths. The indicated frequency value is again approximate due to initial signal distortion. The reasons for the discrepancy between measured signal values and transit time values for different cable lengths are not apparent from the previous theoretical discussion, but may find their basis from a consideration of transmission line properties of two lengths of cable connected across a resistor r. Neglecting effects due to the capacitor, C, and battery resistance, b, one can draw an equivalent circuit, where only components that can effect signal height and transit time are included, as follows:

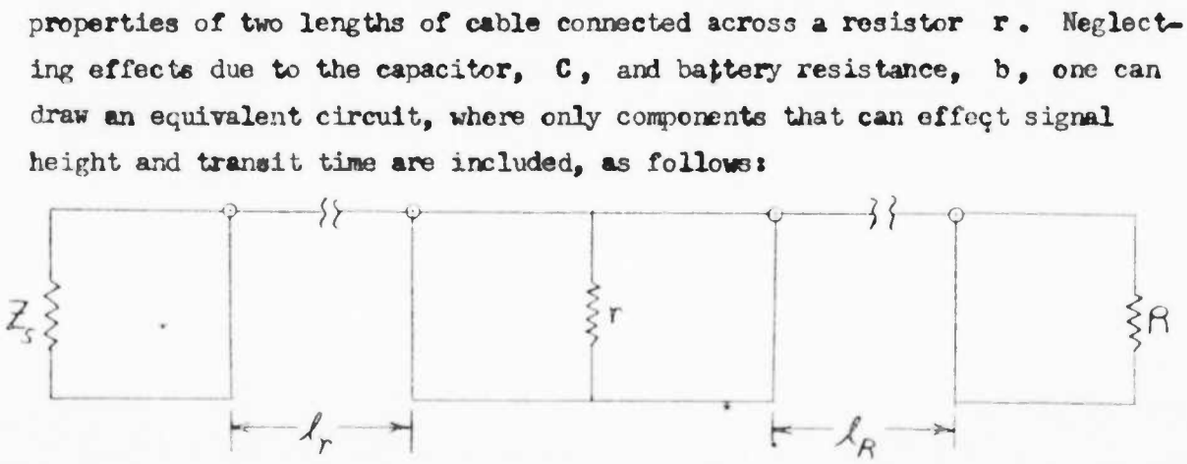

The resistance Z_S represents the input resistance of the oscilloscope plug-in amplifier. This idea has not been worked out in detail but the above does appear to indicate that the transmission line properties of the cable ℓ_r carrying the signal to the oscilloscope can not be ignored.

Since the oscilloscope input resistance is large, the signal cable from the resistor r is poorly terminated at the oscilloscope input terminal. To improve the matching, i.e. reduce the reflection coefficient, k_{z_s}, the signal cable was terminated with a Tektronix type L10-52 ohm matching attenuator at the oscilloscope input terminal. Figure 9 shows the oscilloscope record obtained using this termination.

This mode of operation is effective in eliminating superposed oscillation but other major difficulties are introduced. Since the reflection coefficient, k_{z_s} is not zero the observed signal should contain a number of small voltage steps; these are not seen in Fig. 9. The measured signal voltage is significantly smaller than the calculated signal voltage, e_s. No changes were observed when two different lengths of signal cable, ℓ_r were used. Finally, it was observed when checking the operation of the mercury relay, discussed below, that the use of this termination increases signal response time. The explanation for these effects is not apparent.

(e) Mercury switch operation It is of importance to ascertain that the mercury switch closes cleanly and rapidly so as to eliminate its possible effect upon pulse shape and time duration. The circuitry for observing switch closure is shown below. Figure 10(a) shows the oscilloscope record of the output signal from the 10 ohm resistor upon energizing the mercury

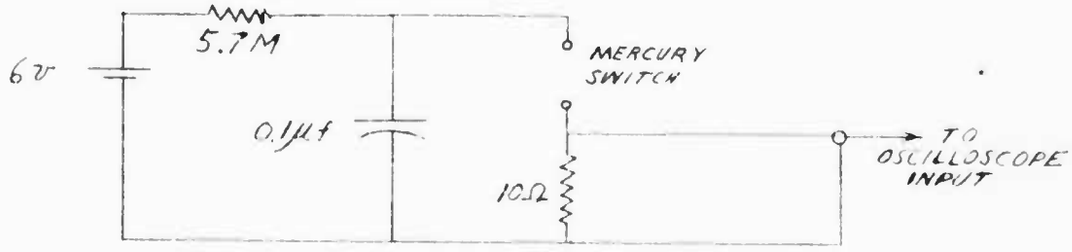

relay. An oscillatory signal is superposed upon the capacitor discharge through the 10 ohm resistor.

The signal rose rapidly from the zero reference to a maximum peak in approximately 0.04 μsec. The oscilloscope rise time is about 0.01 μs. The total rise time of about 0.04 μs compared to the observed time duration of cable pulses of 0.20 μs is satisfactory. For shorter cable lengths, the switch closing time is of the same magnitude as the calculated signal pulse duration time and may account for, in part, the discrepancy between calculated and observed transit time values as noted in Tables V and VI.

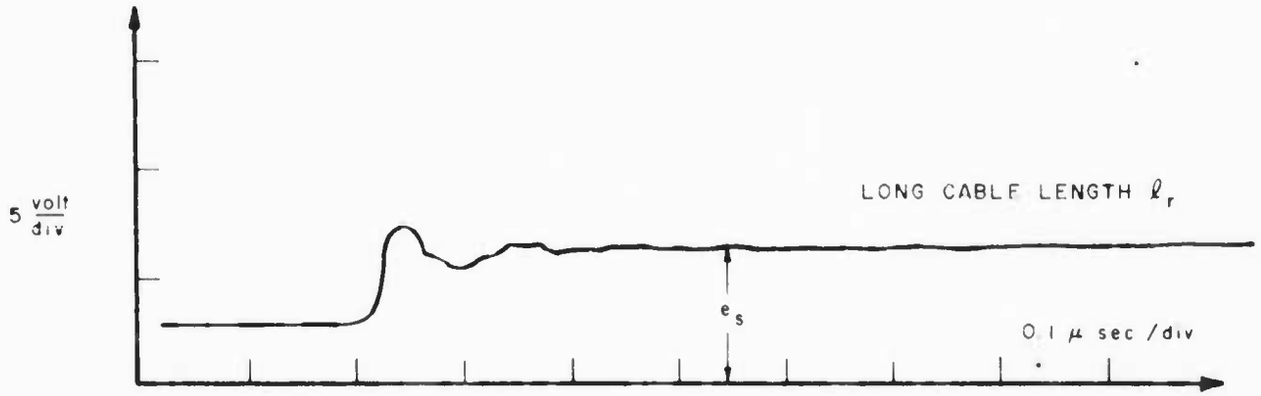

FIGURE 9. TYPICAL SIGNAL RECORD WITH 52 OHM MATCHING ATTENUATOR

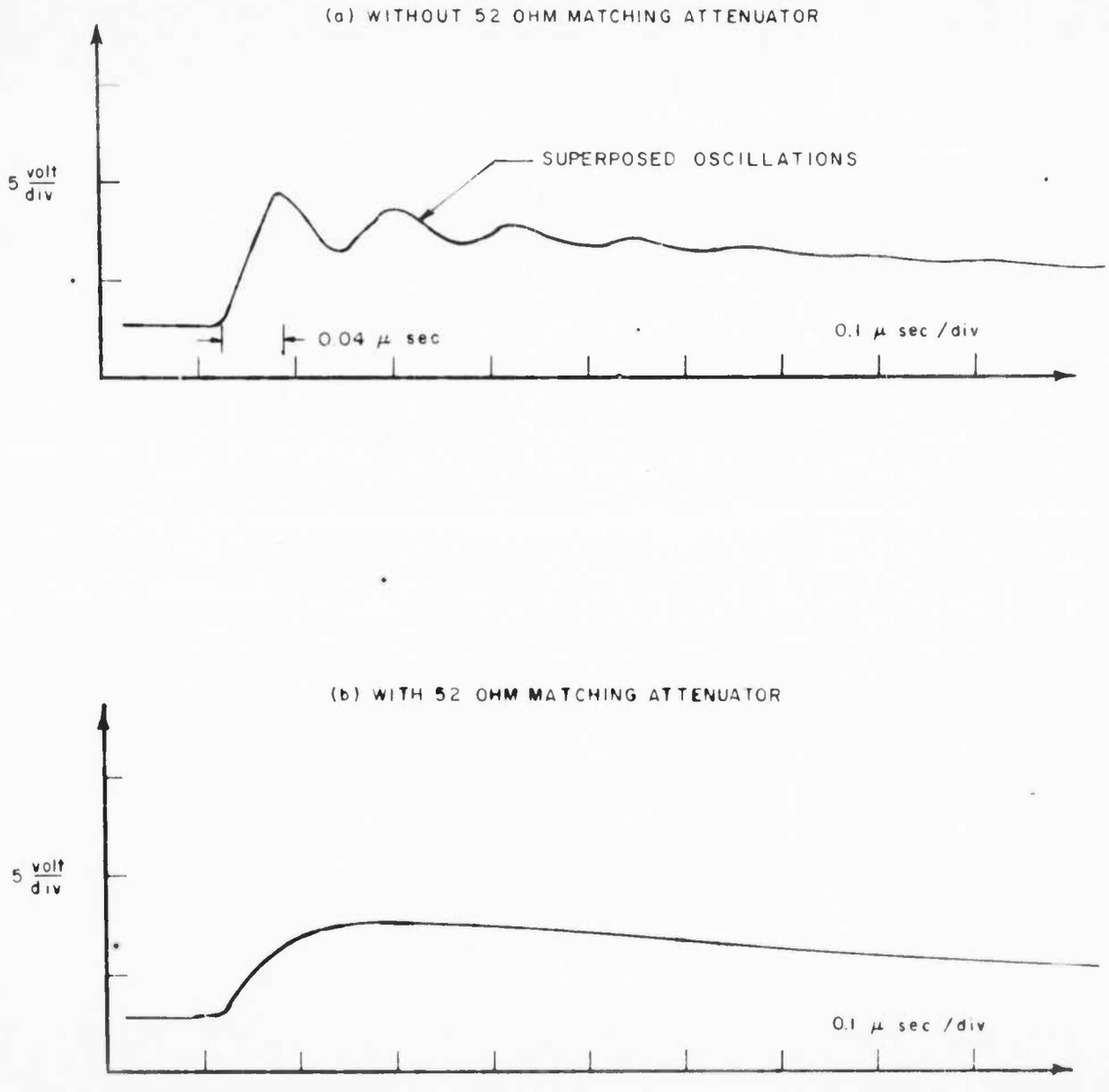

FIGURE 10. RECORD OF MERCURY SWITCH CLOSING CHARACTERISTICS

Figure 10(b) illustrates the effect of using a 52 ohm terminating attenuator at the oscilloscope input terminal resistor. The sharp increase observed with no attenuator is no longer present; the peak signal height now appearing at about 0.10 μsec after initiation. It seems that the use of a 52 ohm terminating attenuator has the detrimental feature of increasing the response time, a poor situation for the time domain of interest here.

(f) Conclusions Summarizing the above results

1. We are able to predict signal height and transit time.
2. One common characteristic observed both in the laboratory and for explosive firings is the presence of an oscillation superposed on the signal. It is felt that this oscillation is high frequency circuit ringing and is unaffected by loading conditions (either fixed resistance or in an explosive environment). Hence the initial signal peak is no direct indication of load value. Its presence in existing instrumentation is unfortunate since much of the information of interest in explosive firings occur in a time period during which oscillations are visible and comparable to pulse signal amplitude.
3. Some important operating features are now clear. To avoid complications due to signal reflections for later periods of time, one should use a properly matched line, i.e. the signal resistor should be equal to the characteristic impedance of the cable. If the signal voltage pulse height can be ascertained, then the results in Fig. 5 can be used to calculate the load.
4. For good sensitivity the signal resistor should be equal to the load resistor.
5. The non-linear variation of signal with load resistance is not a serious drawback of the measuring technique, in view of the accuracy to which signals can be read and other uncertainties introduced by pulse signal distortion due to circuit ringing oscillations and to the uncertainty in the conductivity probe calibration.
6. The use of short lengths of cable does not, by itself, insure improved response time, unless other modifications such as careful wiring and low inductance components are included.

(g) Application of the preceding to the explosive measurement

As was mentioned earlier, the intention of the above discussion and the subsequent laboratory verification is to provide a rational basis for computing probe resistance in an explosive environment. Explosive resistivities are found by measuring the height of the signal voltage observed in a conductivity firing within a time interval given by the round-trip transit

time, 2τ; values of explosive resistance can be read from Fig. 5, or equivalently, calculated from equation (10). Resistivity values are then obtained by means of the individual probe calibration.

Some discussion with regard to the assumptions made concerning detonation zone structure and probe response is required to facilitate interpretation of observed signals. This is necessary since the initial portion of the observed signal contains superposed oscillations and all results will be taken from an average signal voltage over the transit time 2τ. Surface resistance measurements are made with the probe tips so oriented that the detonation front sweeps across the exposed tip area in time. Figure 11 represents an idealized surface conductivity profile for this probe orientation, assuming no extraneous effects induced into the probe's electrical properties due to explosive loading (figure is not drawn to scale). In the absence of superposed oscillations an output signal voltage of similar content would be observed. The output signal is zero until the detonation front reaches the probe (point A) and then increases with time until the detonation zone completely couples the probe (point B). After the detonation zone traverses the probe (point C) the output signal decreases until the zone and probe are no longer linked (point D). Thereafter the output signal is indicative of reaction product conductivity.

For a detonation zone thickness of 1/4 mm, detonation velocity of 7.5 mm/μ sec, and a probe diameter of 0.38 mm, typical values of time are

	time (μ sec)
A to B	0.03
B to C	0.02
C to D	0.03
A to D	0.08

Thus, for surface resistivity measurements, the time period over which the output signal voltage is correlated with detonation zone conductivity is of the order of 0.10μsec.

For comparison, Fig. 12 shows a reproduction of the output signal of firing 28-c, a surface probe measurement. On the faster oscilloscope trace the first observed pulse signal lasts about 0.22μsec, of which the first 0.15μsec is noticeably contaminated with superposed oscillations. Unfortunately the time period over which the observed signal is relatively

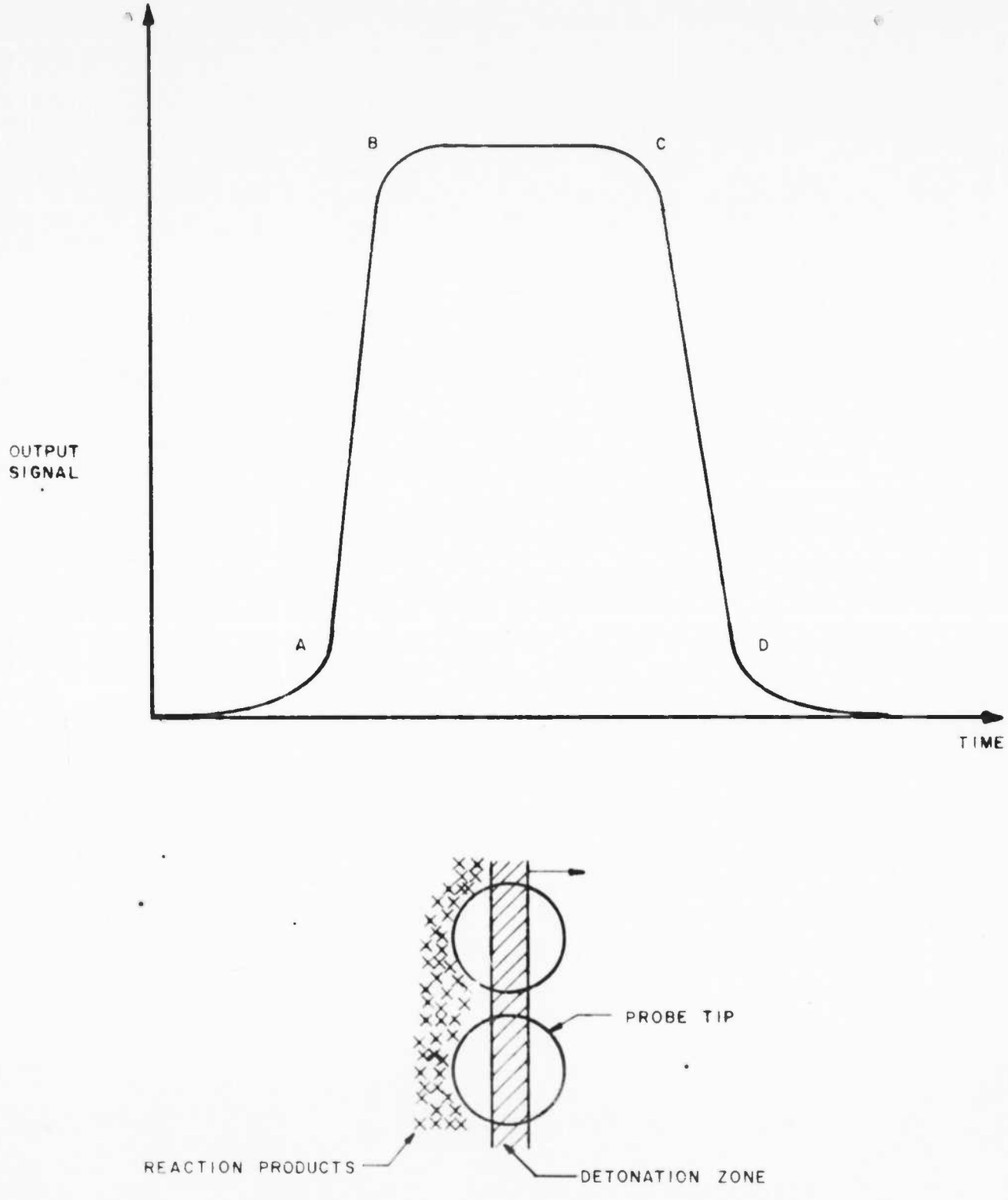

FIGURE II. IDEALIZED CONDUCTIVITY PROFILE AND OUTPUT SIGNAL

free of oscillatory distortion corresponds to a portion of the region, in Fig. 11 from the point D on in time. Thus, measurements of surface resistivity result in values that are possibly more closely related to reaction products than to detonation zone resistivity.

For internal probe measurements the situation is much improved. Since the detonation zone width is larger internally than on the surface, the probe is in the environment of the detonation zone for longer periods of time, for which the superposed oscillations have substantially decayed. For a central reaction zone thickness of 10 mm[2] in an unconfined, cylindrical charge and a detonation velocity of 7.5 mm/μs, typical values of the times are

	time (μsec)
A to B	0.0
B to C	1.25
C to D	0.0
A to D	1.25

(The detonation zone links the probes instantaneously when the probes are head on to the detonation front.)

Figure 13 shows a reproduction of the oscilloscope output signal of firing 39-c, an internal probe measurement. Since the first observed signal pulse lasts about 0.22μs, which is less than 20% of the total time duration, 1.25μs, during which the probe is in the detonation zone, one can calculate a more representative value of detonation zone resistivity. A measure of explosive resistivity, calculated from the second observed signal pulse is of interest since the probe tips are still in the presence of the detonation zone, (at least for the illustrative numbers used above). Resistivity values obtained in this manner will probably include in addition to possible variations of resistivity within the detonation zone, effects of changing probe geometry and extraneous probe effects due to explosive loading.

(h) Calculation of explosive resistivity A summary listing of probe calibration data is presented in Appendix II below, illustrating measured probe resistance, probe calibration values, and calibration error estimates for the number of double probes calibrated to date. The method of

---

(2) R.L. Jameson "Third Symposium on Detonation", Princeton Univ., ONR Report ACR-52 (Sept, 1960)

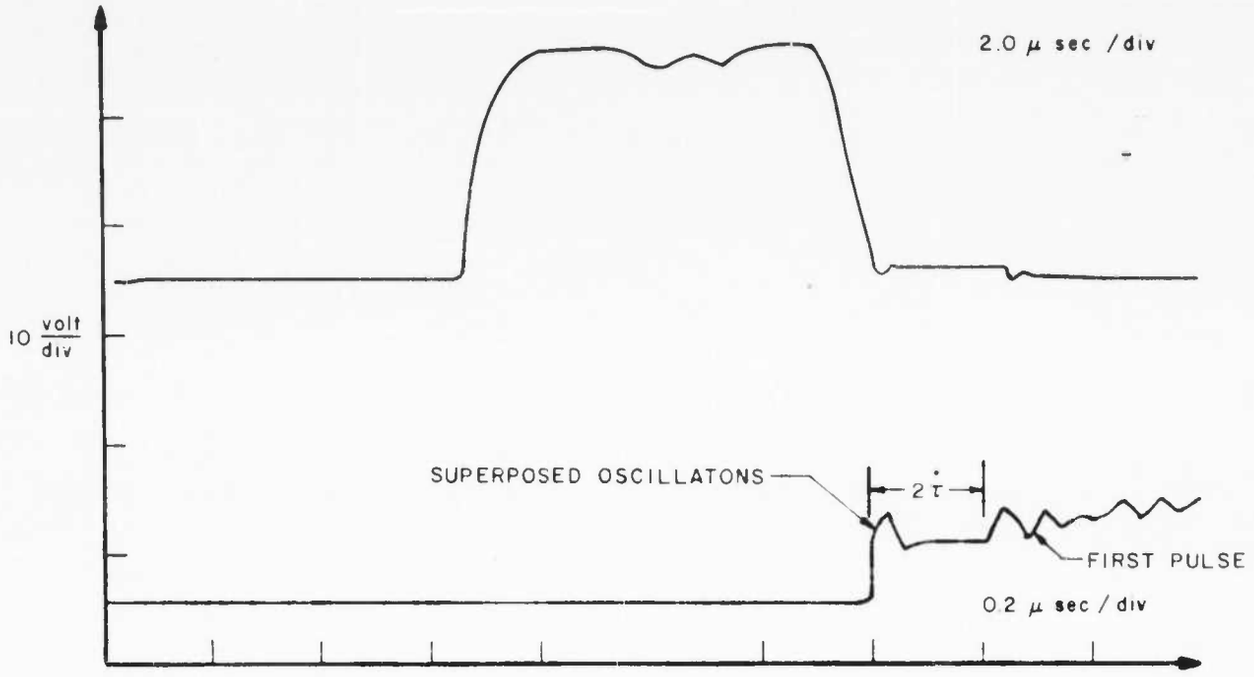

FIGURE 12. OBSERVED SIGNAL FOR A SURFACE PROBE (FIRING 28 – c)

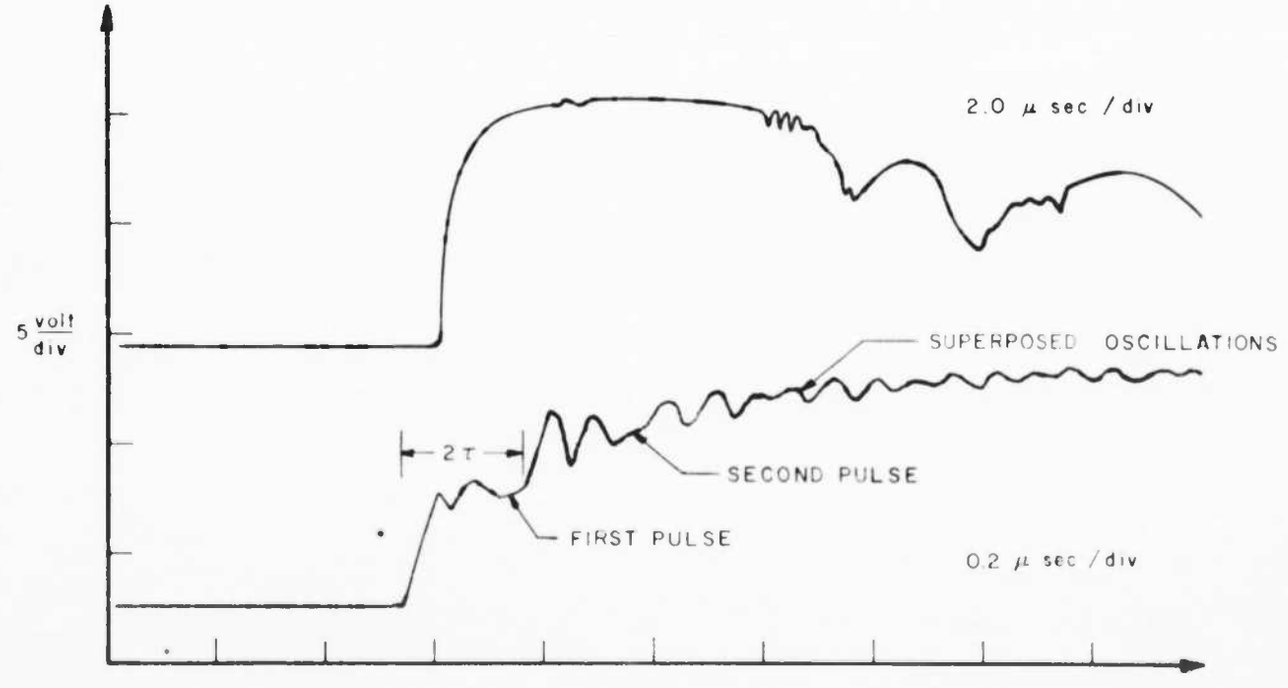

FIGURE 13. OBSERVED SIGNAL FOR AN INTERNAL PROBE (FIRING 39-c)

probe calibration was described in the Quarterly Progress Report October - December 1960.

In light of a new understanding and interpretation of conductivity signals, values of explosive resistivity, incorporating the above mentioned final calibration factors will be presented in the next progress report.

WORK PLANNED FOR NEXT QUARTER

During the next quarter, the assembly of the capacitor bank will be completed. It is expected that testing of the overall bank operation will be underway and measurements of the inductance of the individual elements will be started.

Based on the final probe calibration values presented in this report and the study of the conductivity signal, final explosive resistivities will be reported for all firings to date. This will include a review of each firing in order to select those data for which experimental conditions were optimum and the probe calibrations were satisfactory.

It is also planned to incorporate various improvements in the measuring circuitry as a result of the analysis reported here. These will consist of improving the rise time by rewiring to minimize stray inductance, use of low inductance components, and matching the cable impedance Z_o to the measuring resistance r.

The shaped charge jet collision work will be continued using the lucite vacuum assemblies mentioned in previous progress reports. This will consist of firings in both air and a vacuum. It is planned to make spectrographic observations of the jet interaction region under both conditions.

PERSONNEL

Personnel of Stevens Institute of Technology who have been associated with the work reported here are:

Dr. W.H. Bostick
Dr. S. Koslov
Dr. S.J. Lukasik
Mr. B.J. Pernick
Mr. L.H. Weeks

Personnel of Picatinny Arsenal who have contributed to the work are:

Dr. J.V.R. Kaufmann
Mr. F. Schwartz
Mr. E. Walbrecht
Mr. E. Dalrymple

APPENDIX I

Paper presented at the meeting of the American Physical Society held in New York City, 1-4 February 1961

Electrical Resistivity During a Detonation*

Samuel Koslov, Stephen J. Lukasik, Benjamin J. Pernick
Stevens Institute of Technology
Hoboken, N. J.

Measurements of surface electrical resistivity in the detonation zone of pentolite and composition B have been made. Two probe geometries were employed; one consisted of two copper plates oriented to resemble the letter T, one plate having its flat side against an explosive face, the other plate having its thin edge placed against an opposite face. The second type consisted of two parallel copper wires mounted in a ceramic insulator with the wire ends butted against an explosive face. The resistance of the probe when the detonation zone reaches its edges is measured by recording the transient current under an applied external voltage. The explosive resistivity, ρ, is calculated from the measured resistance, R, using the relation ρ = const. x R. For the T probe this constant is calculated from the known explosive geometry. For the double probe this constant is evaluated by calibration in a material of known conductivity. Resistivity values of the order of 1 ohm cm have been obtained from both probe types. Estimates of the thickness of the reaction zone and the free electron density have been made.

*Work supported by the Ordnance Corp., U.S. Army and carried out in conjunction with Dr. E.N. Clark, Explosives Research Section, Picatinny Arsenal, Dover, N.J.

APPENDIX II

Results of Conductivity Probe Calibration

A total of twenty-six double probes have been calibrated in accordance with the technique described in the Quarterly Progress Report October - December 1960. The numerical results are presented below in Table VII.

The symbols used are:

- h - salt solution depth
- t - generator pulse duration
- R - calculated probe resistance
- ΔR - calculated error estimate for R
- R/ρ - ratio of probe resistance to salt solution resistivity

An applied pulse voltage of 0.1 volt was maintained throughout. This was shown previously[1] to be sufficiently small to eliminate effects due to electrolytic bubble generation on the probe.

For each probe, a linear least squares fit of the dependence of R/ρ on the pulse duration was made for each of the three values of salt solution depth employed; the straight line is represented as

$$R/\rho = \left(\frac{R}{\rho}\right)_o + \text{slope} \times t$$

Figure 14 illustrates a typical variation of the measured values of R/ρ with pulse duration, t, in addition to the best fit straight line for these points, for two typical probes. The zero intercept value $(R/\rho)_o$, is taken to be the probe calibration for the stated salt bath depth. Table VIII lists the results of the straight line fits. Figure 15 is a histogram for all of the values of the intercept $(R/\rho)_o$ and of the slope, obtained in fitting the calibration data to a straight line. No attempt to distinguish salt solution height variability is made since there is no apparent dependence of the ratio $(R/\rho)_o$ upon height. Table IX is a tabulation of earlier preliminary probe calibration results, shown in part previously[1]. These results are not incorporated into the above mentioned figures and tables since the calibration procedure used was not the same.

---

(1) Quarterly Progress Report July - September 1960

Figure 14

Typical probe calibration results

Salt solution depth
- ⊙ 0.047 in.
- \+ 0.072 in.
- ⊡ 0.125 in.

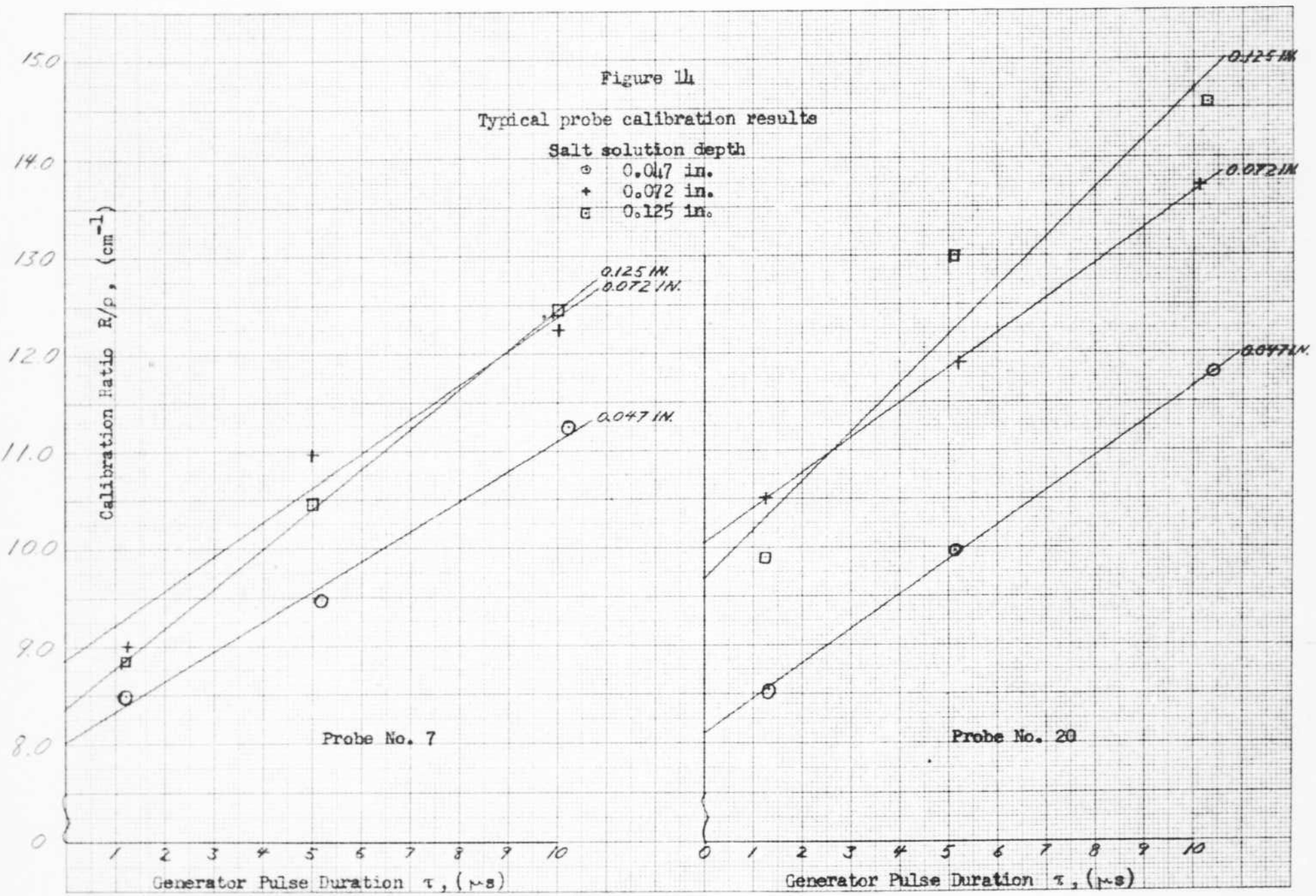

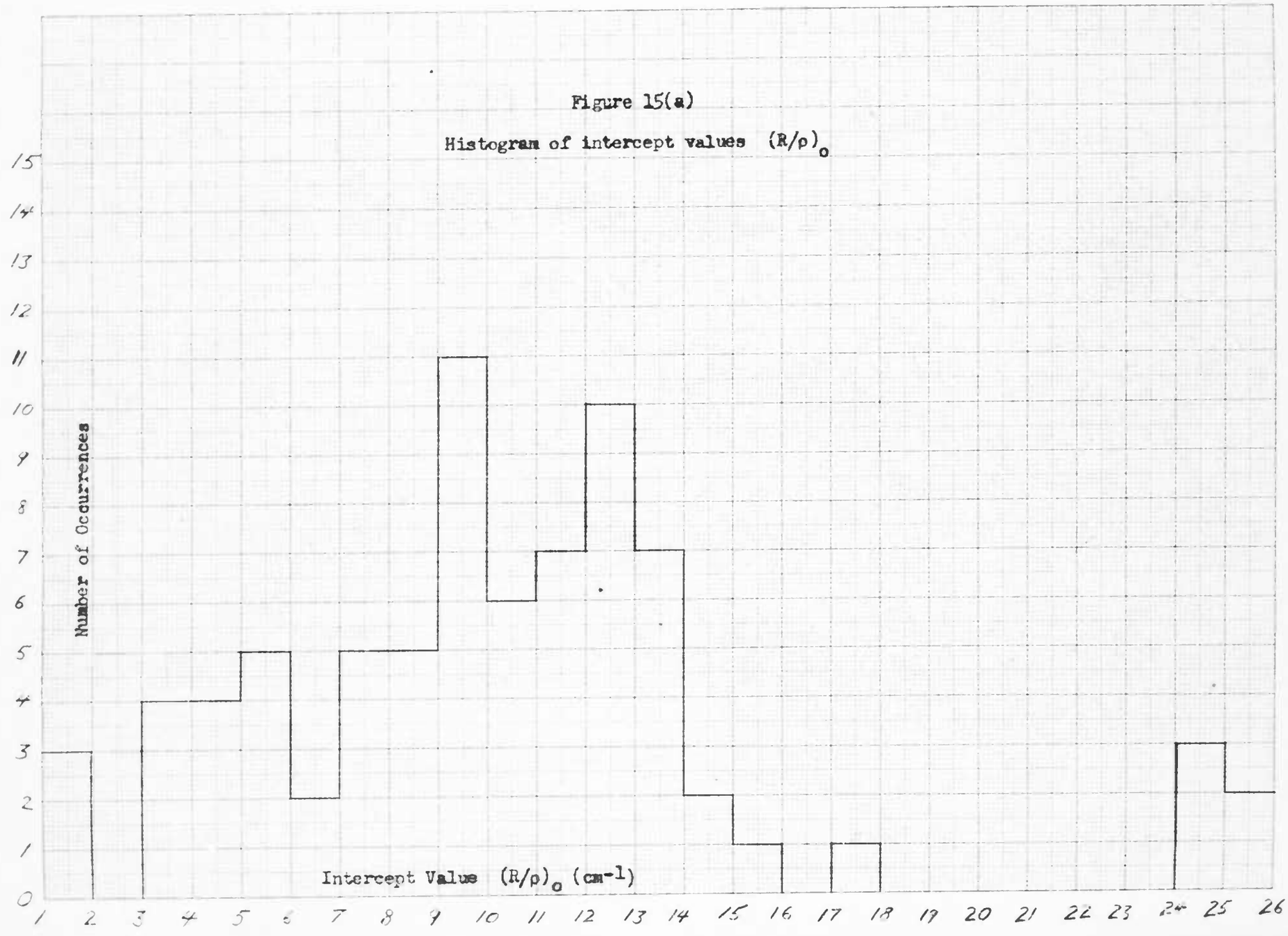

Figure 15(a)

Histogram of intercept values $(R/\rho)_o$

Figure 15(b)

Histogram of slope values

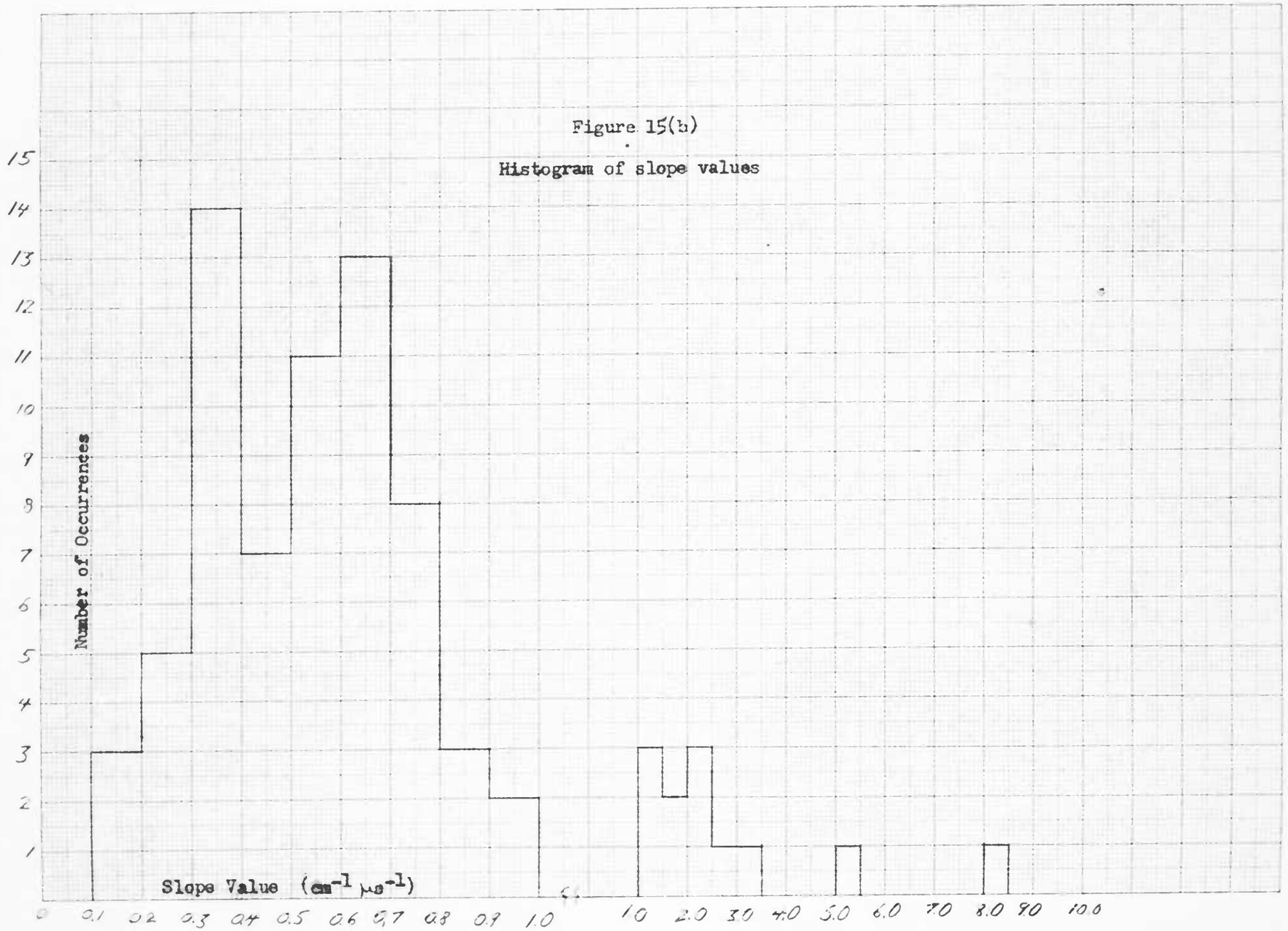

TABLE VII

Probe Calibration Summary

Probe No.	h (inch)	t (μ sec)	R (ohm)	ΔR (ohm)	R/ρ (cm^{-1})
1	0.047	1.08	48.84	12.73	12.54
		4.97	125.65	29.68	32.25
		10.23	652.27	580.25	167.44
	0.072	1.17	68.02	21.67	17.46
		4.95	232.27	70.40	59.62
		10.06	357.76	192.55	91.84
	0.125	1.14	38.82	10.11	9.97
		4.97	82.12	16.90	21.08
		9.94	134.73	34.26	34.58
2	0.047	1.26	21.04	4.98	5.39
		5.16	30.21	3.75	7.75
		9.94	45.99	6.14	11.83
	0.072	1.28	25.39	5.83	6.52
		5.20	31.39	4.42	8.06
		10.04	43.28	6.03	11.11
	0.125	1.27	24.10	6.05	6.19
		4.97	31.69	4.40	8.13
		9.94	40.02	4.75	10.27
3	0.047	1.20	33.31	7.77	8.61
		5.05	45.91	7.31	11.87
		9.90	28.70	5.66	7.42
	0.072	1.24	20.56	5.38	5.33
		5.04	29.19	4.40	7.56
		10.11	56.45	9.85	14.62
	0.125	1.27	20.46	5.55	5.33
		5.06	28.95	4.38	7.54
		10.21	39.05	6.12	10.17
4	0.047	1.26	36.86	7.45	9.66
		5.10	41.07	5.92	10.77
		10.19	48.31	6.31	12.66
	0.072	1.28	37.51	7.63	9.83
		5.14	44.42	5.89	11.64
		10.30	55.60	7.24	14.57
	0.125	1.29	35.53	6.80	9.31
		5.06	40.22	4.06	10.54
		9.96	39.81	4.00	10.43

Table VII (continued)

Probe No.	h (inch)	t (μ sec)	R (ohm)	ΔR (ohm)	R/ρ (cm^{-1})
5	0.047	1.32	36.72	2.88	9.46
		5.06	39.27	1.58	10.11
		10.04	105.83	7.83	27.25
	0.072	1.26	36.78	2.75	9.47
		5.07	39.28	1.51	10.11
		10.11	43.17	1.63	11.12
	0.125	1.31	29.55	2.34	7.59
		5.07	32.46	1.35	8.34
		10.03	36.82	1.54	9.46
6	0.047	1.21	43.21	3.41	11.15
		5.17	54.41	3.00	14.04
		9.91	65.63	3.36	16.93
	0.072	1.34	33.07	2.36	8.55
		5.15	45.84	2.67	11.85
		9.91	52.12	3.05	13.47
	0.125	1.31	66.70	4.94	17.24
		5.02	41.26	1.66	10.67
		10.01	46.18	1.73	11.94
7	0.047	1.21	32.55	2.60	8.47
		5.17	36.43	1.51	9.48
		10.27	43.22	1.65	11.24
	0.072	1.25	34.70	2.72	9.03
		4.98	42.17	1.70	10.97
		10.05	47.11	1.93	12.25
	0.125	1.21	34.04	2.76	8.84
		5.01	40.26	1.67	10.45
		10.01	48.07	2.79	12.48
8	0.047	1.26	32.67	2.71	8.53
		5.09	39.64	1.71	10.35
		10.10	48.50	2.02	12.66
	0.072	1.25	29.04	2.36	7.58
		5.08	38.46	1.64	10.04
		10.28	41.52	1.74	10.84
	0.125	1.25	27.01	2.27	7.05
		5.16	34.62	1.49	9.04
		10.22	45.93	2.23	11.99

Table VII (continued)

Probe No.	h (inch)	t (μ sec)	R (ohm)	ΔR (ohm)	R/ρ (cm^{-1})
9	0.047	1.21	41.49	2.99	10.13
		5.12	47.78	2.54	11.67
		10.14	55.52	2.78	13.56
	0.072	1.24	50.83	3.86	12.36
		5.04	58.30	2.99	14.17
		10.09	63.21	3.14	15.37
	0.125	1.26	50.21	4.04	12.18
		5.17	100.52	5.27	24.39
		10.01	77.11	3.79	18.71
10	0.047	1.42	19.83	0.93	4.87
		5.06	52.69	3.34	12.95
		10.10	65.05	3.45	15.98
	0.072	1.24	51.87	4.19	12.77
		5.13	58.31	3.13	14.36
		10.02	65.79	3.62	16.20
	0.125	1.22	49.28	3.89	12.16
		5.09	58.84	3.05	14.52
		9.95	61.07	3.13	15.07
11	0.047	1.21	43.11	3.14	11.20
		5.09	60.40	3.06	15.69
		10.15	64.17	3.07	16.67
	0.072	1.21	47.78	3.60	11.91
		5.06	63.01	3.20	15.71
		10.06	73.09	3.56	18.22
	0.125	1.23	44.31	3.52	11.00
		5.10	59.05	3.40	14.66
		10.01	67.70	3.80	16.80
12	0.047	1.17	57.62	4.74	13.19
		5.09	84.71	4.22	19.39
		10.10	95.25	4.26	21.80
	0.072	1.13	45.14	3.53	10.38
		5.01	58.28	2.24	13.40
		9.96	63.20	3.26	14.53
	0.125	1.33	42.32	2.92	9.79
		5.10	52.58	2.68	12.17
		9.84	63.65	3.21	14.73

Table VII (continued)

Probe No.	h (inch)	t (μ sec)	R (ohm)	ΔR (ohm)	R/ρ (cm^{-1})
13	0.047	1.24	63.83	4.95	14.97
		5.06	77.82	3.85	18.25
		10.11	88.64	4.31	20.79
	0.072	1.25	59.06	4.49	13.82
		5.07	78.41	4.02	18.35
		10.05	98.75	4.88	23.11
	0.125	1.25	57.23	4.30	13.33
		5.07	71.87	3.70	16.74
		10.14	81.10	3.87	18.89
14	0.047	1.25	61.33	5.13	14.04
		5.06	83.14	4.38	19.03
		9.96	97.10	4.92	22.23
	0.072	1.23	55.54	4.30	12.71
		4.99	70.29	3.59	16.09
		9.98	79.59	3.94	18.22
	0.125	1.23	52.40	4.12	12.02
		5.05	65.55	3.44	15.04
		10.01	79.61	4.04	18.26
15	0.047	1.19	70.61	7.02	16.30
		5.10	86.71	4.17	20.02
		9.90	102.85	4.93	23.75
	0.072	1.19	9.03	0.63	2.09
		5.11	38.66	1.79	8.95
		9.85	36.76	1.63	8.51
	0.125	1.21	9.90	0.69	2.30
		5.09	9.34	0.30	2.17
		9.95	38.01	1.71	8.81
16	0.047	1.20	12.55	0.90	2.94
		4.99	54.33	3.04	12.71
		10.01	46.88	2.44	10.97
	0.072	1.18	13.73	0.96	3.20
		4.96	50.77	2.83	11.86
		9.96	39.66	1.93	9.26
	0.125	1.22	12.04	0.86	2.80
		4.95	9.96	0.35	2.32
		9.90	41.33	2.09	9.63

Table VII (continued)

Probe No.	h (inch)	t (μ sec)	R (ohm)	ΔR (ohm)	R/ρ (cm^{-1})
17	0.047	1.24	9.32	0.69	2.19
		5.04	41.27	2.16	9.70
		10.05	30.03	1.33	7.06
	0.072	1.22	10.08	0.77	2.37
		5.01	41.37	2.33	9.72
		9.98	38.24	1.86	8.99
	0.125	1.26	10.80	0.80	2.54
		5.01	42.24	2.40	9.95
		9.96	37.65	1.97	8.87
18	0.047	1.28	64.59	6.45	13.80
		5.22	42.92	1.71	9.17
		10.20	88.09	4.19	18.82
	0.072	1.21	66.51	6.69	14.21
		5.10	74.10	3.73	15.83
		10.22	93.03	4.47	19.87
	0.125	1.21	66.69	6.52	14.25
		5.06	78.70	3.84	16.81
		10.16	57.60	1.78	12.30
19	0.047	1.31	27.14	2.64	5.82
		5.20	34.58	3.06	7.42
		10.32	42.58	3.42	9.13
	0.072	1.31	27.09	2.67	5.83
		5.17	31.82	1.72	6.84
		10.08	38.15	3.29	8.20
	0.125	1.30	25.06	2.37	5.39
		5.19	31.56	1.73	6.79
		10.05	36.85	3.13	7.92
20	0.047	1.31	39.59	3.80	8.55
		5.13	46.15	2.58	9.97
		10.37	54.66	2.79	11.80
	0.072	1.27	48.68	4.86	10.51
		5.19	55.14	2.81	11.91
		10.14	63.55	3.05	13.73
	0.125	1.25	45.96	4.73	9.90
		5.13	60.36	3.16	13.01
		10.27	67.50	3.16	14.55

Table VII (continued)

Probe No.	h (inch)	t (μsec)	R (ohm)	ΔR (ohm)	R/ρ (cm^{-1})
21	0.047	1.21	45.79	4.26	10.69
		5.26	65.05	3.49	15.19
		10.32	63.48	2.84	14.82
	0.072	1.39	50.28	4.33	11.71
		5.13	60.80	3.04	14.16
		10.38	68.19	3.27	15.88
	0.125	1.30	52.29	4.47	12.15
		5.19	58.69	2.85	13.64
		10.47	66.01	3.05	15.34
22	0.047	1.34	130.50	13.88	28.70
		5.09	110.66	5.43	24.33
		10.51	265.62	28.08	58.41
	0.072	1.29	128.21	13.89	28.45
		5.18	153.37	8.74	34.03
		10.38	208.63	12.43	46.29
	0.125	1.24	131.65	15.94	29.41
		5.18	178.24	11.73	39.82
		10.40	232.86	15.03	52.02
23	0.047	1.34	46.56	5.04	10.61
		5.29	55.18	2.85	12.58
		10.33	70.97	3.98	16.17
	0.072	1.15	57.31	5.89	13.03
		4.61	60.68	2.92	13.80
		10.58	72.63	3.91	16.52
	0.125	1.17	48.00	5.50	10.84
		5.31	66.25	3.51	14.96
		10.66	69.78	2.99	15.76
24	0.047	1.19	57.10	5.40	13.53
		5.28	60.73	2.58	14.39
		10.56	68.39	2.88	16.21
	0.072	1.23	55.31	5.39	13.14
		5.29	61.15	2.66	14.52
		10.57	71.68	3.04	17.02
	0.125	1.20	55.86	4.79	13.29
		5.24	62.60	2.75	14.90
		10.53	69.55	2.94	16.55

Table VII (continued)

Probe No.	h (inch)	t (μ sec)	R (ohm)	ΔR (ohm)	R/ρ (cm^{-1})
25	0.047	1.27	58.98	6.01	14.22
		5.29	70.07	3.39	16.89
		10.88	487.94	134.46	117.64
	0.072	1.28	59.83	4.79	14.43
		5.37	77.69	3.83	18.73
		10.64	89.64	5.32	21.61
	0.125	1.29	59.50	5.42	14.32
		5.52	77.27	4.51	18.59
		10.84	112.84	7.57	27.15
26	0.047	1.24	108.46	13.38	26.43
		5.41	140.22	8.81	34.17
		10.74	181.59	13.62	44.25
	0.072	1.25	110.61	12.63	27.09
		5.26	150.12	11.52	36.76
		10.59	196.64	15.10	48.16
	0.125	1.20	93.18	9.88	22.82
		5.30	98.14	6.57	24.04
		10.63	177.01	11.79	43.35

TABLE VIII

Linear Least Squares Fit to Probe Calibrations

Probe No.	h (inch)	Slope ($cm^{-1}\mu sec^{-1}$)	Intercept $(R/\rho)_o$ (cm^{-1})	Final Disposition
1	0.047	5.06	7.06*	Firing No. 26-c
	0.072	8.25	11.85	
	0.125	2.79	6.93	
2	0.047	0.74	4.27	Sent to BRL
	0.072	0.53	5.65	
	0.125	0.47	5.67	
3	0.047	0.85	7.58*	Sent to BRL
	0.072	1.07	3.34	
	0.125	0.54	4.71	
4	0.047	0.34	9.16	Firing No. 27-c
	0.072	0.53	9.07	
	0.125	0.12	9.43	
5	0.047	0.17	9.25*	Firing No. 38-c
	0.072	0.19	9.21	
	0.125	0.21	7.29	
6	0.047	0.66	10.44	Firing No. 40-c
	0.072	0.56	8.20	
	0.125	0.26	9.38*	
7	0.047	0.31	8.02	Firing No. 39-c
	0.072	0.36	8.79	
	0.125	0.41	8.35	
8	0.047	0.47	7.95	Cast, not fired
	0.072	0.35	7.56	
	0.125	0.55	6.30	
9	0.047	0.38	9.68	Cast, not fired
	0.072	0.32	12.14	
	0.125	0.67	14.75	
10	0.047	0.59	9.97*	Cast, not fired
	0.072	0.39	12.31	
	0.125	0.32	12.16	
11	0.047	0.59	11.28	Cast, not fired
	0.072	0.70	11.46	
	0.125	0.65	10.60	
12	0.047	0.94	12.98	Firing No. 28-c
	0.072	0.46	10.31	
	0.125	0.58	9.09	

Table VIII (continued)

Probe No.	h (inch)	Slope ($cm^{-1}\mu sec^{-1}$)	Intercept $(R/\rho)_o$ (cm^{-1})	Final Disposition
13	0.047	0.65	14.46	Firing No. 29-c
	0.072	1.05	12.69	
	0.125	0.62	12.94	
14	0.047	0.93	13.41	Firing No. 32-c
	0.072	0.62	12.33	
	0.125	0.71	11.26	
15	0.047	0.85	15.43*	Firing No. 31-c
	0.072	0.74	1.21*	
	0.125	0.75	1.40*	
16	0.047	0.84	4.31	Firing No. 33-c
	0.072	0.63	4.73*	
	0.125	0.79	1.84*	
17	0.047	0.50	3.61	Firing No. 30-c
	0.072	0.71	3.19	
	0.125	0.68	3.45	
18	0.047	0.62	10.46	Firing No. 34-c
	0.072	0.64	13.12*	
	0.125	0.67	13.44*	
19	0.047	0.37	5.40	Broken, not fired
	0.072	0.27	5.46	
	0.125	0.29	5.11	
20	0.047	0.36	8.10	Firing No. 23-c
	0.072	0.36	10.05	
	0.125	0.50	9.69	
21	0.047	0.43	11.15	Broken, not fired
	0.072	0.46	11.35	
	0.125	0.35	11.75	
22	0.047	3.24	24.34*	Firing No. 35-c
	0.072	1.98	25.12	
	0.125	2.46	26.62	
23	0.047	0.62	9.60	Firing No. 36-c
	0.072	0.38	12.38	
	0.125	0.50	10.99	
24	0.047	0.29	13.08	Cast, not fired
	0.072	0.42	12.51	
	0.125	0.35	12.95	

TABLE IX

Preliminary Probe Calibration Summary*

Probe No.	Applied Voltage (v)	t (μsec)	R (ohm)	R/ρ (cm^{-1})	Final Disposition
40	0.1	2.18	13.30	3.56	Broken
		3.93	27.47	7.35	
		5.98	20.13	5.38	
		8.21	46.38	12.40	
		10.10	45.80	12.25	
41	0.1	0.48	21.33	5.42	Firing 19-c
		1.26	14.04	3.86	
		2.14	16.35	4.49	
		4.06	21.51	5.91	
		6.17	21.07	5.79	
		8.36	29.92	8.22	
		10.14	31.85	8.75	
	1.0	0.46	21.83	5.54	
		1.23	13.12	3.61	
		2.10	15.61	4.29	
		3.83	21.55	5.92	
		5.91	20.38	5.60	
		8.28	28.37	7.79	
		10.29	26.08	7.17	
	10.0	0.44	23.81	6.04	
		1.09	48.23	13.25	
		2.17	66.49	18.27	
		3.89	81.36	22.35	
		5.89	69.22	19.02	
		8.09	75.21	20.66	
		10.23	64.38	17.69	
	25.0	1.23	31.24	8.58	
		2.11	41.64	11.44	
		3.92	80.76	22.19	
		5.99	88.48	24.31	
		8.39	147.10	40.42	
		10.00	158.55	43.56	
42	0.1	0.45	15.65	3.97	Firing 14-c
	1.0	0.46	14.24	3.61	
	10.0	0.44	14.21	3.60	
43	0.1	0.46	13.95	3.56	Firing 15-c
	1.0	0.46	12.95	3.31	
	10.0	0.44	13.16	3.36	
44	0.1	0.46	159.10	40.97	Firing 16-c
	1.0	0.48	163.24	42.04	
	10.0	0.46	164.23	42.29	

*A salt solution depth of 0.125 in. used throughout.

Table IX (continued)

Probe No.	Applied Voltage (v)	t (μsec)	R (ohm)	R/ρ (cm^{-1})	Final Disposition
45	0.1	0.47	294.19	76.67	Firing 17-c
	1.0	0.49	333.18	86.83	
	10.0	0.50	298.08	77.68	
46	0.1	0.51	205.01	53.86	Firing 18-c
	1.0	0.50	197.80	51.96	
	10.0	0.47	198.67	52.19	

DISTRIBUTION LIST

Commanding Officer
Diamond Ordnance Fuse Laboratories
Washington 25, D. C.

Technical Reference Section (1)

Commanding General
Aberdeen Proving Ground
Aberdeen, Maryland

BRL - Dr. R. Eichelberger (1)

Chief of Ordnance
Department of the Army
Washington 25, D. C.

ORDTB (1)

Armed Services Technical Information Agency
Arlington Hall Station
Arlington 12, Virginia (10)

Commanding Officer
Picatinny Arsenal
Dover, New Jersey

Purchasing Office, ORDBB-PB1 (5)

Commanding Officer
Office of Ordnance Research
Box CM, Duke Station
Durham, North Carolina

Dr. Sherwood Githen (1)

Explosives Research Laboratory
Bureau of Mines
4800 Forbes Avenue
Pittsburgh 13, Pennsylvania

Dr. F. Gibson (1)

Carnegie Institute of Technology
Pittsburgh, Pennsylvania

Dr. F. Allison (1)

Mr. Laddie L. Stahl
Manager - Technical Relations
General Electric Company
Schenectady, New York (1)

Dr. Arthur H. Guenther
Director, Pulse Power Laboratory
Air Force Special Weapons Center
Kirtland Air Force Base
New Mexico (1)

Dr. David Bernstein
Poulter Laboratories
Stanford Research Institute
Menlo Park, California (1)